Afterglow effect in photoluminescence of Si:Er

M. Forcales and T. Gregorkiewicz
Van der Waals–Zeeman Institute, University of Amsterdam, Valckenierstraat 65, NL-1018 XE Amsterdam, The Netherlands

I. V. Bradley and J-P. R. Wells
FOM Institute for Plasma Physics "Rijnhuizen," P.O. Box 1207, NL-3430 Nieuwegein, The Netherlands and Department of Physics, Heriot Watt University, Edinburgh EH14 4AS, United Kingdom

(Received 27 November 2001; revised manuscript received 19 February 2002; published 7 May 2002)

The afterglow effect of slowly decaying photoluminescence, well known for phosphor materials, is identified in silicon. A component with a lifetime of up to 100 ms is observed in kinetics of the $\lambda \approx 1.5$ μm emission of Er-doped crystalline silicon. This is measured at $T \approx 4.2$–40 K under pulsed band-to-band excitation with a Nd:YAG laser (532 nm). The slow component is found to be superimposed upon the Er-related emission characterized by the commonly reported lifetime of approximately 1 ms. Thermalization and subsequent recombination of nonequilibrium carriers trapped at shallow levels after the excitation pulse is proposed as the microscopic mechanism responsible for this slow emission. Using time-resolved two-color spectroscopy with a free-electron laser, the earlier reported mid-infrared induced enhancement of Er emission is related to the presently observed afterglow. A simple kinetic model is developed and shown to successfully link the amplitude and temporal characteristics of both effects. Measurements at higher temperatures support the proposed interpretation.

DOI: 10.1103/PhysRevB.65.195208 PACS number(s): 78.55.Ap, 61.72.Tt, 41.60.Cr

I. INTRODUCTION

Rare earth (RE) doped semiconductors are very attractive systems for photonic applications. In particular, Er^{3+} intra-$4f$-shell luminescence features sharp emission at an almost temperature independent wavelength of 1.5 μm, which falls at the minimum loss of optical fibers used in telecommunications. Silicon, the leading material for electronics, is not very suitable for optoelectronic applications due to its indirect band gap. However, since the first observation of low temperature 1.54 μm emission from a Si:Er material,[1] much effort has been invested to realize a fully integrated room-temperature optoelectronic device based on Si:Er. Unfortunately, weak emission intensity is the major drawback. Two possible mechanisms are usually held responsible for the poor room-temperature emission. As the temperature increases, either excitation efficiency decreases, and/or nonradiative recombination processes (Auger) become more important. Previous work[2–6] indicated that only deeper understanding of nonradiative recombination processes will lead to the realization of efficient room temperature Er emission. In the past, temperature and excitation power dependence of steady-state photoluminescence (PL) of differently prepared Si:Er materials was extensively investigated. However, with increasing temperature or excitation density many processes are activated simultaneously and this can obscure observation of the energy transfer paths in the excitation and deexcitation of Er^{3+} ions. Consequently, very little information can be derived from these nonselective experiments. Much better results can be obtained with a free electron laser (FEL) as a tunable source in the midinfrared (MIR). In this case, we can precisely address specific centers involved in the excitation and the deexcitation of Er^{3+} ions.[7] In the earlier work[8] we have observed that following a primary band-to-band excitation by a Nd:YAG laser, Er PL could be enhanced by a MIR radiation pulse. In the present contribution we identify a slowly decaying component of Er PL at 1.54 μm (the afterglow). Using the time-resolved two-color spectroscopy with the FEL, we establish a relation between this slow PL component and the temporal characteristics of the MIR-induced Er PL enhancement.

II. EXPERIMENTAL DETAILS

In the current research, samples with different erbium and oxygen concentrations have been investigated. While the amplitude and the temporal characteristics of the $\lambda \approx 1.54$ μm emission change somewhat from one sample to another, the general behavior and the effects produced by the FEL are common for all of them. The data presented in this paper were obtained for a Si:Er sample prepared from Czochralski-grown *p*-type silicon. Er ions were implanted with an energy of 300 keV to a dose of 3×10^{12} cm^{-2}. The concentration of erbium in the implanted layer was around 5×10^{17} cm^{-3}. The sample was coimplanted with oxygen ions with an energy of 40 keV to a dose of 3×10^{13} cm^{-2}. Oxygen codoping is known to increase intensity of Er PL and to reduce its thermal quenching. The implantation was followed by 900 °C annealing during 30 min. A high resolution PL spectrum obtained from the sample under Ar^{+} laser excitation is plotted in the inset to Fig. 1. In the spectrum we can identify several lines related to transitions from the $^4I_{13/2}$ multiplet of Er^{3+} to the crystal field split $^4I_{15/2}$ ground state. A similar spectrum is also observed under pulsed excitation with a Nd:YAG laser. In the experiment the sample is placed in a helium gas flow variable temperature cryostat (Oxford Instruments Optistat) allowing measurements in the temperature range from 4.2 to 300 K. Excitation of the Er^{3+} ions is provided by a frequency doubled pulsed Nd:YAG laser (532 nm). Er PL is dispersed through the spectrometer (Triax 320

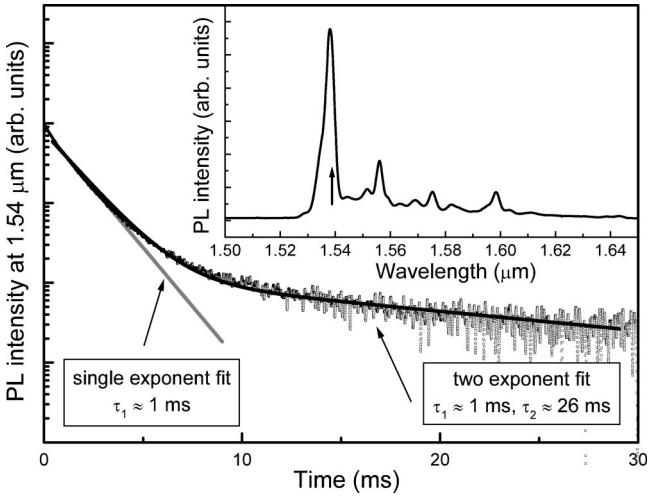

FIG. 1. Decay kinetics of Er PL excited by a Nd:YAG laser pulse, measured with a PMT at $T=4.2$ K. A good fit can be obtained with a double exponent function with time constants $\tau_1 \approx 1$ ms and $\tau_2 \approx 26$ ms. In the inset, high resolution PL spectrum measured under Ar^+ ion laser excitation is shown. Several lines split by crystal field can be observed. The most intense line used for investigations of the dynamics is marked with an arrow.

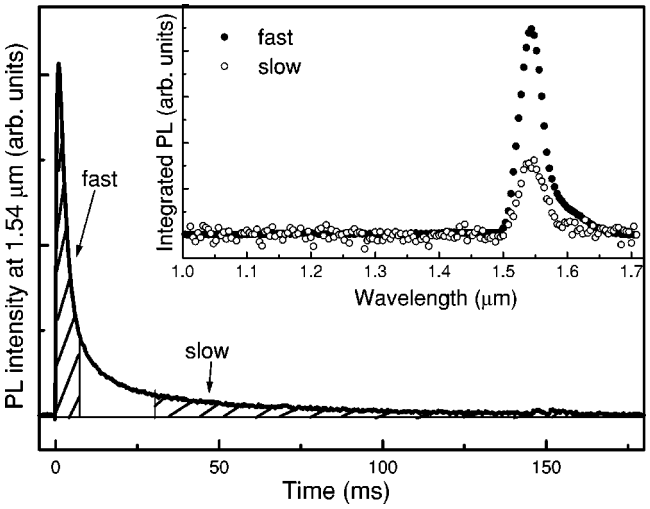

FIG. 2. Spectral dependence of the slow and the fast components of the Er PL ($T=4.2$ K). The inset shows amplitude of the PL signal integrated in the indicated time windows. See text for further explanation.

or Yobin Ivon THR 1500). For detection we use either a sensitive Ge photodiode (Edinburgh Instruments, EI-A) for slowly decaying signals and also for spectral analysis, or an infrared sensitive photomultiplier tube (Hamamatsu Photonics, R5509-72) to capture fast signals. The PL transients are fed into a digital oscilloscope (TDS 3032, Tektronix). The experimental time resolution of the system is $\tau_{det} \approx 30$ μs. In the case of two-color experiments a FEL pulse, spatially overlapped on the sample with the Nd:YAG, is fired after a selected delay time. For more details on the experimental set-up for two-color spectroscopy with the FEL see, Refs. 7,8.

III. EXPERIMENTAL RESULTS

A. Photoluminescence kinetics

Figure 1 shows decay kinetics of the Er-related PL signal measured with a PMT at $T=4.2$ K under excitation with the second harmonic of the Nd:YAG laser, and an excitation density of approximately 30 μJ/cm^2 per pulse. Since all the lines in the inset of Fig. 1 show identical kinetics, in order to get the best signal-to-noise ratio we choose the line with the highest intensity for detailed investigations (marked with an arrow in the inset). Unfortunately, lifetime measurements can only be performed with a lower resolution. In that case only a broad line centered at $\lambda \approx 1.54$ μm is detected . As can be seen, the Er PL signal with the usually reported decay time of approximately $\tau_1 \approx 1$ ms is superimposed on a much slower decaying background. This is more evident in Fig. 2, which illustrates the same kinetics as Fig. 1, but with the time scale extended to 180 ms. In the inset to the Fig. 2, spectral characteristics of the fast and the slow components are shown. These were obtained by integrating PL signal over time windows between 1 and 8 ms for the fast, and 30 and 150 ms for the slow components, respectively, as indicated in the figure. The characteristic spectrum of Er^{3+} is clearly reproduced in both cases. The simultaneous appearance of two Er related PL components with different decay characteristics raises a question as to their individual contributions to the total emission. An investigation of the excitation power dependence of both components shows that the slower component dominates for small excitation densities. Upon increasing the excitation density, the slow component saturates, while the faster one continues to grow. Its eventual saturation level depends on the particular sample preparation conditions, but is always much higher than that of the slower one. The different saturation behavior of both Er PL components is illustrated in Fig. 3, where kinetics obtained for two

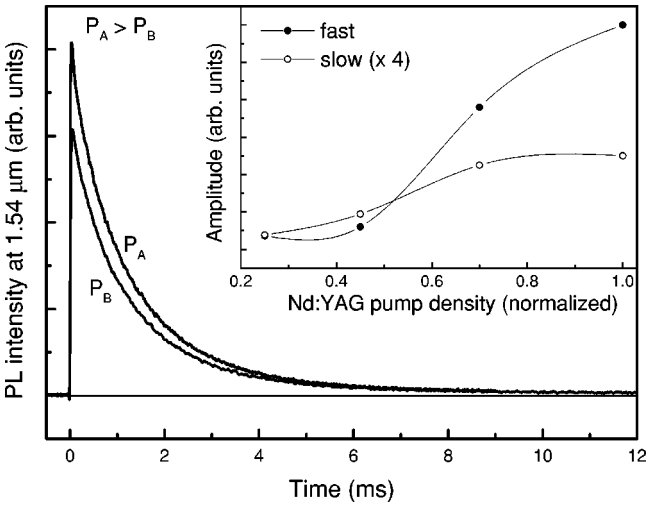

FIG. 3. Er PL dynamics detected with a PMT at $T=4.2$ K for two different pump power densities. The inset shows power dependences of the slow and the fast components. As can be seen, the amplitude of the slow component saturates earlier. The solid lines are to guide the eye.

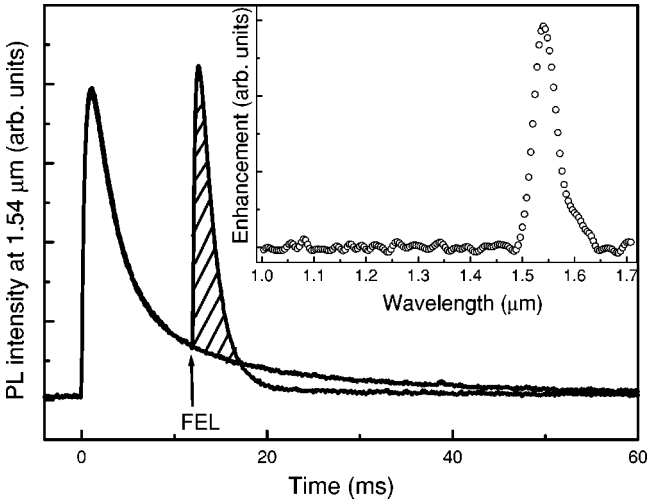

FIG. 4. Illustration of the MIR-induced PL enhancement observed at $T=4.2$ K and detected with a Ge detector. FEL pulse ($\lambda_{FEL}=10$ μm) was fired with a delay of $\Delta t=12$ ms after Nd:YAG laser. In the inset, spectral characteristics of the MIR-induced PL is shown: the marked area under the curve is plotted as a function of the emission wavelength. The MIR-induced PL is clearly related to Er emission.

different excitation densities are compared. As can be concluded from the inset, the PL signal characterized by a shorter $\tau_1 \approx 1$ ms decay time increases with excitation power, while the slow one reaches saturation and its intensity remains constant.

B. Two-color experiments in the MIR

A FEL pulse applied within several tens of milliseconds after the initial band-to-band excitation leads to an enhancement of Er-related emission.[8] While the magnitude and the time scale of this effect is sample dependent, the MIR-induced enhancement is found to be omnipresent for all Er-doped crystalline silicon. It is illustrated in Fig. 4 for low intensity visible excitation. A FEL pulse at $\lambda_{FEL}=10$ μm was applied with a delay of 12 ms. In order to establish whether the enhancement effect is exclusively related to Er PL, the spectral dependence of the integrated FEL-induced signal (marked in the figure) was measured. The result, depicted in the inset to the figure, shows that additional emission appears only at the Er-characteristic wavelength around $\lambda_{Er}=1.54$ μm. From Fig. 4 we also note that, in contrast to the earlier discussed Er PL excited by a band-to-band pump pulse, the MIR-activated Er PL contains only the fast-decaying component with $\tau_1 \approx 1$ ms. At the same time, the enhancement of the fast signal is accompanied by a clear quenching of the slow one. Figure 5 illustrates how the magnitude of the effect depends on the delay time between the FEL and the pump pulses, under conditions of high [Fig. 5(a)], and low [Fig. 5(b)] pump excitation density. The different signal rise time in both figures is related to the different detector used for the two excitation regimes. Insets to both figures show kinetics of the enhancement effect. As can be seen, under conditions of strong pumping the amplitude

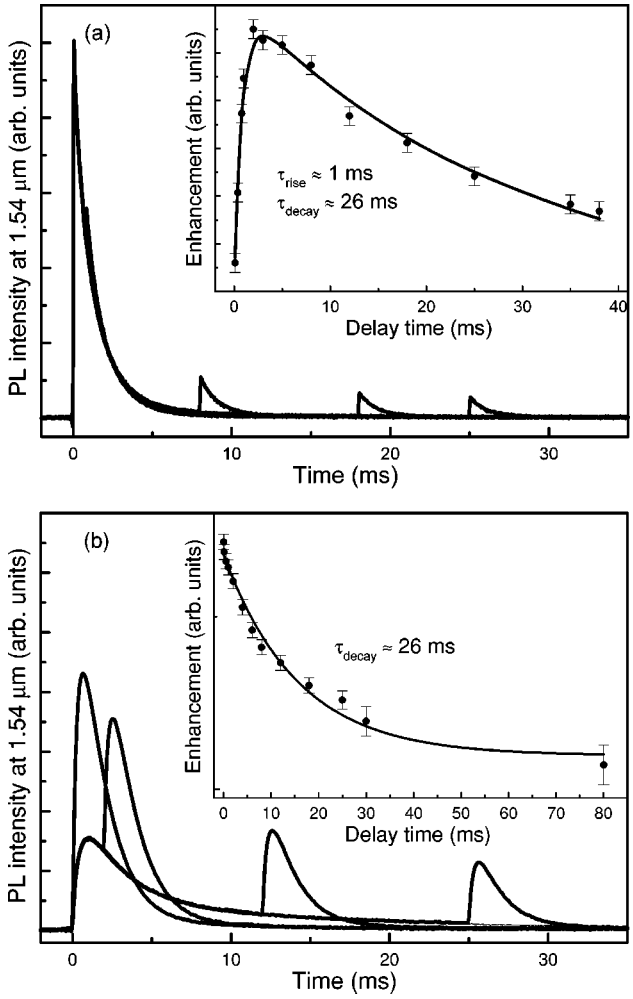

FIG. 5. Temporal characteristics of the MIR-induced Er PL enhancement under high (a) and low (b) pump power densities, respectively. The inset shows the amplitude of the enhancement effect as a function of the delay time. For a high power the magnitude of the enhancement shows a rise time of $\tau_{rise} \approx 1$ ms, while for a low power an immediate enhancement is observed. The enhancement effect disappears always with the same decay time constant $\tau_{decay} \approx 26$ ms. Measurements are taken at $T=4.2$ K using PMT and the Ge detector, for the high and the low excitation power regimes, respectively.

of the MIR-induced PL gradually increases for short delay times, reaches a maximum, and subsequently decreases with a very large time constant. For weak pumping, the enhancement effect sets in immediately, and then decreases with the same time constant as for the strong pumping case. The MIR-induced enhancement effect of the Er PL is not a linear process, as depicted in Fig. 6, where it is illustrated for different pulse energies of the FEL for a wavelength of $\lambda_{FEL}=8$ μm. Experimentally this was achieved by placing attenuators in the FEL beam. From the inset to the figure we conclude that saturation is reached within the available power range. We also note that the magnitudes of the enhancement of the fast component of the PL signal and of the quenching of the slow one are mutually related. When the enhancement is saturated, the slow component is completely removed.

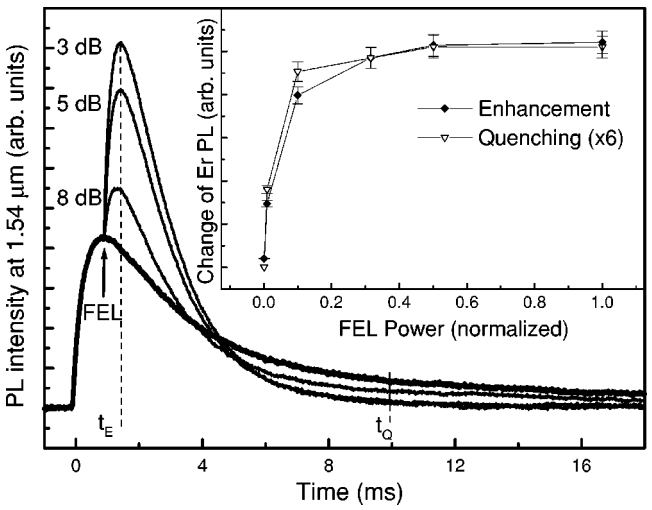

FIG. 6. The effect of FEL pulse energy (three different settings) on the amplitude of the MIR-induced Er PL enhancement ($\lambda_{FEL}=8$ μm, $\Delta t=1$ ms, $T=4.2$ K, Ge detector). In the inset, power dependence of the enhancement and the quench amplitude (measured at $t_E \approx 1.8$ ms and $t_Q \approx 10$ ms, respectively) are compared. The mutual relation of both effects is evident.

Finally, influence of lattice temperature on the MIR-induced Si:Er PL was investigated. The effect of the FEL pulse applied with a fixed delay at three different temperatures is depicted in Fig. 7. The intensity of the initial PL response to the pump pulse has been normalized for clarity of comparison. We note that the relative contribution to the total PL signal of the slow component decreases at higher temperatures, and so does the amplitude of the FEL-activated emission. At a temperature of approximately 40 K Er PL enhancement is almost absent.

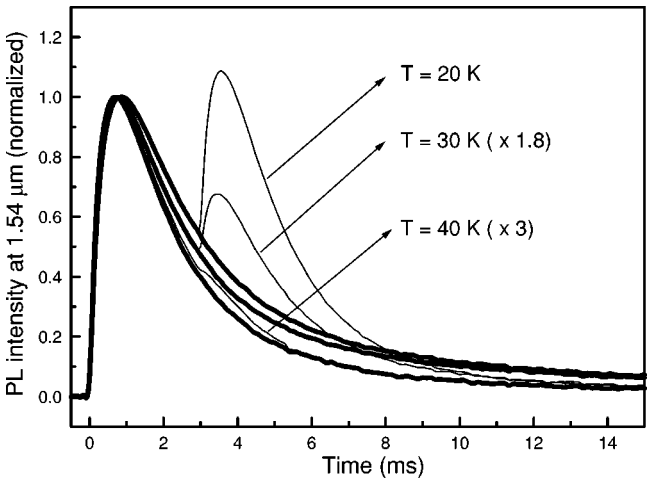

FIG. 7. MIR-induced Er PL at different temperatures. The PL intensity has been normalized for clarity. The afterglow and the MIR-induced Er PL enhancement effect disappear gradually upon temperature increase.

IV. DISCUSSION

A. Preliminaries

The photoluminescence intensity is proportional to the number of emitting centers, in our case Er^{3+} ions in the excited state, divided by the radiative decay time

$$I_{PL} \alpha \frac{N_{Er}^*}{\tau_{rad}}. \quad (1)$$

In the ideal case, when photon emission is the only recombination path, it is possible to determine precisely the excited state lifetime from PL kinetics. However, it is commonly found that nonradiative deexcitation paths are simultaneously present, shortening the excited state lifetime. The effective decay time (τ_{eff}) will result from a combination of radiative (τ_{rad}) and nonradiative (τ_{nrad}) processes, $\tau_{eff}^{-1} = \tau_{rad}^{-1} + \tau_{nrad}^{-1}$. Both components are entangled and difficult to separate. We note, that when the excitation is turned off the relative importance of individual mechanisms of nonradiative recombination could vary with time, thus leading to a time dependent form of τ_{eff}. At low temperatures radiative recombination is dominant, but nonradiative processes become more important with increasing temperature. In the research on Si:Er we have to take into account several mechanisms of nonradiative recombination. The Auger process is one of them. Electrons/holes in the conduction/valence band thermally ionized from shallow traps interact strongly with Er^{3+} ions in the excited state.[5] Due to the fact that nonradiative relaxation is an intrinsically fast process, we usually have $\tau_{nrad} < \tau_{rad}$. These parallel recombination paths can be activated thermally, but will also appear under conditions of high pump density. Due to presence of free carriers, the kinetics will show a fast initial decay and a shortening of the entire lifetime.[3] Similarly, under continuous illumination, an equilibrium concentration of free carriers in the band will interact with Er^{3+} ions. After the excitation is switched off, the Auger effect, which is directly related to the concentration of carriers, will change with time. At higher temperatures, another nonradiative deexcitation mechanism, the so-called "back transfer" process,[5,9] will further hamper Er PL. The back transfer was first proposed for the InP:Yb system[10] and later adopted for Si:Er. The main idea is that by absorbing phonons the excitation process is reversed and the energy is transferred from Er^{3+} ions in the excited state $(Er^{3+})^*$ back to the intermediate stage. In addition to these processes, a possibility of nonradiative recombination by multiphonon relaxation is sometimes considered, as well as energy migration between individual Er-related centers, provided that their concentration is sufficiently high. Experimentally, the exchange of energy between centers will lead to a stretched exponent character of the PL kinetics[11,12] as common for random processes.

Surprisingly few reports are available on the Er PL dynamics at cryogenic temperatures. It has been observed that Er forms a variety of different optically active centers,[13] showing clearly different PL spectra. However, similar decay time constants were observed for all of them.[14] In contrast to the above, small lifetime differences are reported for Er in

differently prepared samples (e.g., different host materials, different implantation energies, annealing treatment, etc.). Such differences are probably due to different non-radiative processes active in these materials.

B. Kinetics of Er^{3+} PL signal

The simplest function which gives a good agreement with the experimental trace depicted in Fig. 1 is a double exponential decay $I_{PL}=A_1\exp[-(t-t_0)/\tau_1]+A_2\exp[-(t-t_0)/\tau_2]$. From a fit starting at $t_0\approx 300$ μs to avoid the influence of the detector response time, we have determined two lifetimes: a fast component of $\tau_1\approx 1$ ms and a very slow component of $\tau_2\approx 26$ ms with a ratio of $A_2/A_1\approx 0.025$. We identify $\tau_1\approx 1$ ms as the lifetime of the Er ions in the first excited state $^4I_{13/2}$, as commonly assumed[2,9] and will denote it further as τ_{Er}. We note that this τ_{Er} is clearly shorter than the estimated purely radiative recombination time $\tau_{rad}\approx 20$ ms.[15] Microscopic identification of the slow component is less straightforward. The slow component has a small amplitude and is difficult to detect using a short time window; consequently it is easy overlooked in an experiment. The slow component was observed in all the samples investigated here and disappears at temperatures above 40 K. Its amplitude and lifetime were sample dependent varying between 20 and 100 ms. More information about the slow component can be found in Fig. 2, where the time-resolved spectrum is shown. To analyze whether the slow emission has a specific wavelength dependence, spectra for the fast and the slow component were experimentally separated. The signal amplitude integrated over the time window from 1 to 8 ms contains in the major proportion the $\tau_1\approx 1$ ms component, while the amplitude integrated from 30 to 150 ms carries only information on the slow component. As can be seen in the inset to the figure, within our spectral resolution, both components have the same spectral response as in the inset of Fig. 1 and are therefore uniquely related to emission from Er^{3+} ions. The pump excitation density can also be used to separate the two components. In Fig. 3 we show kinetics of PL intensity at 1.54 μm for two different pump powers. The slow component saturates at a lower power than the fast one, as shown in the inset. For very low excitation densities, PL signal is dominated by the slow component.

C. Mathematical description of excitation and deexcitation processes

As a first approximation of the problem we consider that the two PL components identified in the kinetics arise from two independent contributions superimposed at the Er^{3+} characteristic wavelength of $\lambda=1.54$ μm. The simplest way to describe the phenomenon is to relate the two lifetime values to recombination of two types of Er-related centers, e.g., erbium ions in two different environments. The rate equations for the system will have the following form:

$$\frac{dN_{e\text{-}h}}{dt}=G\,\delta(t)-\frac{N_{e\text{-}h}}{\tau_0}, \tag{2}$$

$$\frac{dN^*_{Er1}}{dt}=C_1N_{e\text{-}h}(N^{total}_{Er1}-N^*_{Er1})-\frac{N^*_{Er1}}{\tau_{Er1}}, \tag{3}$$

$$\frac{dN^*_{Er2}}{dt}=C_2N_{e\text{-}h}(N^{Total}_{Er2}-N^*_{Er2})-\frac{N^*_{Er2}}{\tau_{Er2}}, \tag{4}$$

where $N_{e\text{-}h}$, N^*_{Er1}, N^*_{Er2}, and τ_0 denote the number of electron-hole pairs, the number of erbium ions in the excited state from the species 1 and 2, and the effective lifetime of electron-hole pairs, respectively. A short band-to-band excitation pulse by the Nd:YAG laser $[\delta(t)]$ will create electron-hole pairs in the system ($N_{e\text{-}h}$) with generation rate $G\,\delta(t)$. The number of electron-hole pairs will decrease exponentially from the solution of Eq. (2). An effective time constant of τ_0 will predominantly indicate a nonradiative process, since radiative recombination of electron-hole pairs in silicon has a low probability. In the literature we find several mechanisms for Er^{3+} optical excitation: an electron from an Er-related level recombining with a hole in the valence band,[4] a free exciton bound at an Er-related level forming an intermediate state of a bound exciton character,[16] or a resonant excitation via a Δ_2' conduction subband[17] among others. The common feature for all of them is that nonradiative recombination of at least two particles transfers energy to the $4f$ shell of the Er^{3+} ions. Therefore in our description we consider erbium excitation by electron-hole pair recombination with energy transfer in an Auger process to the $4f$ shell. Because the two PL components have different amplitudes and can saturate (Fig. 3), we introduce individual capture coefficients (C_1 and C_2), lifetimes (τ_{Er1} and τ_{Er2}), and saturation terms (N^{total}_{Er1} and N^{total}_{Er2}) for the two kinds of centers. Once we have solved Eqs. (3) and (4), taking into account the initial conditions $N^*_{Er1}(t=0)=0$ and $N^*_{Er2}(t=0)=0$, we superimpose both signals keeping in mind Eq. (1). In that way good agreement with the experimental PL dynamics can be obtained. Following the excitation pulse, the PL signal initially rises with a time constant determined by the electron-hole pair lifetime, and then decays with τ_{Er} and τ_2.

While such a mathematical description of the experimental results is correct, we note that according to our findings, the decay time of the slow component changes from sample to sample (20–100 ms range) and its microscopic origin is not clear. Moreover, there is no particular justification for the existence of only two different optically active Er centers, and not more.

D. Microscopic origin of the slow PL signal

Until now we have considered that the excitation mechanism of Er^{3+} ions by an intermediate state, in our description assumed to be an electron-hole pair, was fast, i.e., $\tau_0<\tau_{Er},\tau_2$. This assumption can indeed be supported from Fig. 1. In the depicted kinetics recorded with a fast PMT detector, we do not find any real rise time, which in the assumed excitation model, should correspond to the effective energy transfer time to the $4f$ shell. The experimentally observed rise time of the signal reflects the detector response time. We

recall that fast energy transfer was also postulated by Taguchi *et al.*,[18] using the same type of detector.

We will now consider here another kind of intermediate state, with a very slow Er pumping rate, in order to explain the appearance of the slow component. Let us suppose that following band-to-band excitation one kind of emitting erbium centers is excited through an intermediate state, labeled *A*. The relevant rate equations will be

$$\frac{dA}{dt} = -\frac{A}{\tau_{\mathrm{tr}}}, \tag{5}$$

$$\frac{dN_{\mathrm{Er}}^{*}}{dt} = \frac{A}{\tau_{\mathrm{tr}}} - \frac{N_{\mathrm{Er}}^{*}}{\tau_{\mathrm{Er}}}, \tag{6}$$

where τ_{tr} is the time for energy transfer from *A* to the erbium ions. The PL intensity I_{Er} from the solution of Eqs. (5) and (6), with the initial conditions that $A(t=0)=A_0$ (we assume the instantaneous creation of the intermediate state) and $N_{\mathrm{Er}}^{*}(t=0)=0$ will be

$$I_{\mathrm{Er}} = \frac{A_0}{(\tau_{\mathrm{Er}}-\tau_{\mathrm{tr}})}\left[\exp\left(-\frac{t}{\tau_{\mathrm{Er}}}\right) - \exp\left(-\frac{t}{\tau_{\mathrm{tr}}}\right)\right]. \tag{7}$$

Using a fixed value of the Er decay time $\tau_{\mathrm{Er}} \approx 1$ ms, we will consider this solution for $\tau_{tr} \ll \tau_{\mathrm{Er}}$ and for $\tau_{\mathrm{tr}} \gg \tau_{\mathrm{Er}}$. If $\tau_{\mathrm{tr}} \ll \tau_{\mathrm{Er}}$, the signal will rise with the transfer time and will decay with $\tau_{\mathrm{Er}}(\approx 1$ ms), as expected. When the transfer time is very fast (nanosecond scale) then the detector response time constant will control the rise of I_{Er}, as seen in Fig. 1. We note that a similar situation will occur when the lifetime of the intermediate state *A* is affected by an alternative recombination process (τ_{alt}). In such a case Eq. (5) will change to

$$\frac{dA}{dt} = -\frac{A}{\tau_{\mathrm{tr}}} - \frac{A}{\tau_{\mathrm{alt}}} = -\frac{A}{\tau_{\mathrm{tr}}^{\mathrm{eff}}}. \tag{8}$$

If the transfer to N_{Er}^{*} is of a μs scale and the nonradiative recombination not leading to Er^{3+} excitation is characterized by a τ_{alt} of a few ns, the resulting $\tau_{\mathrm{tr}}^{\mathrm{eff}}$ will be of the same order of magnitude. The experimentally observed I_{Er} will rise very fast, while the real transfer time to the Er^{3+} ions will be much slower.

An interesting situation occurs when the transfer time is longer than the lifetime of Er: $\tau_{\mathrm{tr}} \gg \tau_{\mathrm{Er}}$. In this specific case I_{Er} will rise with a $\tau_{\mathrm{Er}} \approx 1$ ms time constant and decay with τ_{tr}. We can therefore explain the experimentally measured kinetics of Er PL as a superposition of signals generated via fast and slow intermediate states, with the contribution from the fast one being much bigger than that from the slow one. The time constant of $\tau_{\mathrm{Er}}=1$ ms will represent the lifetime of Er in the excited state, while the time constant of $\tau_2 = 26$ ms will reflect a slow excitation time and not a slow recombination process. Such a slow excitation process could be realized by thermal release of free carriers generated by the band-to-band laser pulse and captured at shallow traps. Indeed, a short band-to-band pulse will create free carriers whose recombination will excite Er^{3+} ions in a fast Auger process. These will subsequently emit with the characteristic decay time of $\tau_{\mathrm{Er}} \approx 1$ ms. However, free carriers will also be captured at traps, whose origin can be related to implantation damage or to impurity contamination of the host. The probability of recombination of nonequilibrium carriers captured at traps involves their thermal emission to the band and is small at low temperatures. The thermal emission rate *R* of trapped carriers,[19] depends on temperature and the trap ionization energy E_{trap}:

$$R = N_B \sigma \langle v \rangle = 10^{11} \exp\left(-\frac{E_{\mathrm{trap}}}{k_B T}\right), \tag{9}$$

where N_B (N_C,N_V), $\langle v \rangle$, and σ are the density of states in the (conduction/valence) band, the average thermal carrier velocity and a ionization coefficient, respectively. Taking a typical energy of the effective mass theory shallow trap in Si to be $E_{\mathrm{trap}} \approx 45$ meV, we obtain that the lifetime of a nonequilibrium trap is around 30 ms for a temperature of $T \approx 20$ K and lowers below ~ 1 μs for $T \geqslant 45$ K. We propose that the slow component ($\tau_2 \approx 26$ ms) appearing in Er PL is due to excitation of Er^{3+} ions by recombination of carriers thermally released from traps with carriers of the opposite type available at the Er-related recombination centers. Such a mechanism resembles very much the afterglow effect, well known for phosphor materials used in optoelectronics,[20] but to our knowledge, never before been reported for silicon. The proposed identification is supported by results obtained for the same material in two-color spectroscopy in the mid-IR, as discussed in the next section.

E. MIR-induced Er PL enhancement

In the earlier work,[8] we investigated the MIR-induced Er PL enhancement effect as a function of the energy of the incident photons. Based on those studies, we concluded that ionization of carriers from shallow traps was responsible for the effect, with the wavelength dependence of the ionization cross section[21] forming a fingerprint of the involved traps. In this contribution we have further investigated temporal characteristics of the enhancement PL, in order to establish its possible link with the afterglow effect reported here for the Si:Er material.

In Fig. 4 we show the Er PL enhancement effect as observed for low pump intensities at a delay $\Delta t = 12$ ms between the visible and FEL pulses. The MIR radiation set at $\lambda_{\mathrm{FEL}} = 12$ μm is attenuated by 8 dB in order to avoid saturation. As can be seen, under these conditions the amplitude of the MIR-induced PL signal is comparable to that of the signal generated by the band-to-band primary excitation. The dynamics of the FEL-induced PL is similar to the fast component observed in Fig. 1 and assigned to the decay of Er^{3+} ions τ_{Er}. The identification of the extra PL as the Er^{3+} emission is also supported by the spectral dependence indicated in the inset of the figure. This shows that the enhancement appears exclusively at the characteristic erbium wavelength of $\lambda = 1.54$ μm. The temporal behavior of the enhancement effect is depicted in Figs. 5(a) and 5(b) for high and low pump densities, respectively. As reported earlier,[22] in Fig. 5(a) the additional Er PL cannot be seen for short delays

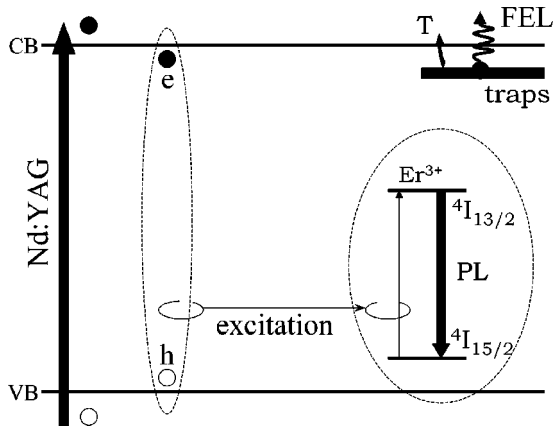

FIG. 8. Microscopic model of the afterglow and the MIR-induced Er PL effects. Trapping of electrons has been assumed for purpose of illustration of the mechanism. For a detailed explanation see text.

($\Delta t < 1$ ms). The effect appears for longer delay time values and diminishes on a ~ 10 ms time scale. This is shown by the fitting illustrated in the inset to Fig. 5(a), where we have used the same parameters as found for the slow and the fast components in Fig. 1. Good agreement is obtained.

The gradual increase of the MIR-induced PL is difficult to explain if we assume that ionization of nonequilibrium shallow traps is responsible for the enhancement. Capture of nonequilibrium carriers by traps in silicon is fast and therefore their ionization by the FEL should be possible immediately after the pump pulse. This is clearly not the case. However, under pulsed excitation conditions it is easily possible to saturate the Er PL, as seen in Fig. 3. Figure 5(b) shows the MIR-induced enhancement effect measured under low excitation density, using the Ge detector for a better sensitivity. In this case, the incubation time of 1 ms is no longer present, while the enhancement effect disappears with a decay time that has the same value as in Fig. 5(a). The observation of a rise time in Fig. 5(a) can now be explained by saturation of the Er PL by the visible pulse. The MIR-induced enhancement decays with a lifetime of 26 ms which is the same as obtained for the afterglow effect in the fit illustrated in Fig. 1. It is possible to ionize the traps at any time, but the magnitude of the effect will be proportional to the actual number of populated traps. For short delay times between the two laser pulses, the traps will have the maximum number of carriers and the enhancement effect will be large. As the delay time is increased, the number of carriers will decrease due to the thermalization and the magnitude of enhancement effect will gradually reduce. In that way the enhancement and the afterglow effects are mutually related. This is further supported by observation of a clear quench of the afterglow luminescence which follows the Er PL enhancement—see Figs. 4 and 5(b). A quantitative description of the relation of both components is given in the next section.

F. Microscopic model

In Fig. 8 we schematically illustrate the microscopic model proposed to explain the origin of the observed effects. After band-to-band excitation by a Nd:YAG pulsed laser, Er^{3+} ions are excited by an Auger recombination of electron-hole pairs. Parallel to this process, free carriers are captured at shallow traps. In the cartoon, these are depicted as electron traps, but from our data we cannot conclude whether electron or hole traps are involved in the proposed mechanism. We further assume that recombination of the trapped carriers and return to equilibrium proceeds mainly via their thermal re-emission to the band. This process will provide an additional channel of slow excitation for the Er^{3+} ions. Since excitation of Er^{3+} requires recombination of two carriers of opposite types, we assume that the second carrier is captured at an Er-related center immediately after the visible laser pulse. Alternatively to thermalization, carriers can be optically released from the traps by the FEL pulse, giving rise to an abrupt increase of the Er PL, detected as a MIR-induced enhancement effect. For the sake of completeness, we note that bound excitions (BE's) readily formed in Si at low temperatures, cannot be responsible for the enhancement effect due to their short lifetime ($\sim$ns for donor/acceptor BE or $\sim$ up to 100 μs for isoelectronic BE).

The mathematical model of the proposed process is very similar to Eqs. (2)–(4). N^*_{Er2} is now replaced by N^*_{traps} being the number of filled traps, τ_{Er2} by a thermalization time τ_{traps}, and $N^{\mathrm{total}}_{\mathrm{Er2}}$ by the total number of available traps $N^{\mathrm{total}}_{\mathrm{traps}}$. At the time when the FEL is fired at the sample (t_{FEL}) ionization occurs. We consider a new generation term G_{FEL} which is proportional to the number of traps filled at that moment ($t = t_{\mathrm{FEL}}$):

$$G_{\mathrm{FEL}} = qN^*_{\mathrm{traps}}(t_{\mathrm{FEL}}). \tag{10}$$

The factor q represents the efficiency of the ionization process and its value will vary between $0 < q \leqslant 1$ depending on the ionization cross section (σ) and the flux of MIR photons (ϕ), $q \,\alpha\, \phi\sigma$. The new set of rate equations describing the system after the FEL pulse, i.e., for $t' \geqslant t_{\mathrm{FEL}}$ will be

$$\frac{dN_{e\text{-}h}}{dt'} = G_{\mathrm{FEL}}\delta(t') - \frac{N_{e\text{-}h}}{\tau_0}, \tag{11}$$

$$\frac{dN^*_{\mathrm{Er}}}{dt'} = C_1 N_{e\text{-}h}(N^{\mathrm{total}}_{\mathrm{Er}} - N^*_{\mathrm{Er}}) - \frac{N^*_{\mathrm{Er}}}{\tau_{\mathrm{Er}}}, \tag{12}$$

$$\frac{dN^*_{\mathrm{traps}}}{dt'} = C_2 N_{e\text{-}h}(N^{\mathrm{total}}_{\mathrm{traps}} - N^*_{\mathrm{traps}}) - \frac{N^*_{\mathrm{traps}}}{\tau_{\mathrm{traps}}}, \tag{13}$$

where $t' \epsilon (t_{\mathrm{FEL}}, \infty)$. The initial conditions will be $N^*_{Er}(t' = t_{\mathrm{FEL}}) = N^*_{\mathrm{Er}}(t_{\mathrm{FEL}})$ and $N^*_{\mathrm{traps}}(t' = t_{\mathrm{FEL}}) = 0$ if all the traps are ionized by the FEL pulse. In Fig. 9 we show that for a fixed delay time, a simulation using the above model [Eqs. (11)–(13)] can reproduce the experimental data very well. We note, that in order to reproduce results obtained with a slow detector, e.g., the FEL-induced enhancement depicted in Fig. 4, the kinetic changes obtained as solutions to Eqs. (11)–(13) have to be convoluted with the detector response time. Also in such a case (not shown), perfect agreement with the experiment is obtained, thus supporting the proposed model and its assumptions.

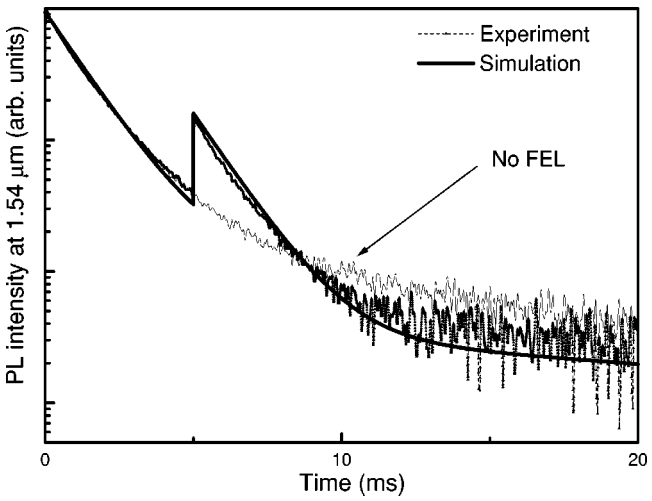

FIG. 9. Comparison of experimental data on the FEL-induced PL with a simulation by the kinetic model based in Eqs. (11)–(13). As can be seen, the enhancement of Er excitation and the accompanying quench of the afterglow are well reproduced ($\lambda_{FEL}=10\mu$m, $\Delta t=5$ ms, $T=4.2$ K, PMT detector).

The microscopic model linking the FEL-induced excitation of Er and the thermal depopulation of nonequilibrium traps available in the host is further confirmed by experiments at higher temperatures. This is illustrated in Fig. 7 where the dynamics of the Er PL is shown for $T=20$, 30, and 40 K. As the temperature rises, nonradiative processes gain in importance. Consequently, the amplitude of the Er PL will be lower. In Fig. 7 the PL intensity has been normalized: in that way decrease of the afterglow and of the amplitude of the enhancement effect can clearly be seen. This is due to an increase of the thermal emission rate at higher temperatures, and a faster return to equilibrium. We can observe that the afterglow and the FEL-induced enhancement effects disappear simultaneously and are no longer present at $T>45$ K. This confirms mutual relation of both effects and evidences also shallow character of traps responsible for carrier trapping and storage.

V. CONCLUSIONS

Based on the presented results obtained at cryogenic temperatures we conclude that recombination of carriers, released thermally from nonequilibrium traps available in silicon and populated by a visible pump pulse, is responsible for an afterglow effect of the slowly decaying component of Er PL. Further, by two-color spectroscopy with a free-electron laser, we show that the MIR-induced enhancement effect of the Er PL results from optical ionization of the same shallow centers. A link between the afterglow effect and the MIR-induced Er PL enhancement is conclusively established. As the temperature increases, the magnitudes of both effects diminish, as thermalization of trapped carriers accelerates. A simple kinetic model is proposed and shown to give excellent account of the experimentally measured amplitude of the Er PL enhancement for different delay times.

ACKNOWLEDGMENTS

We acknowledge Professor Dr. W. Jantsch for providing Si:Er material used in this study. Numerous discussions with Dr. M. S. Bresler and Dr. O. B. Gusev are deeply appreciated. The work was financially supported by the European Research Office (ERO) and the Nederlandse Organisatie voor Wetenshappelijk Onderzoek (NWO).

[1] H. Ennen, J. Schneider, G. Pomrenke, and A. Axmann, Appl. Phys. Lett. **43**, 943 (1983).
[2] L. C. Kimerling, K. D. Kolenbrander, J. Michel, and J. Palm, Solid State Phys. **50**, 333 (1997).
[3] S. Coffa, G. Franzò, F. Priolo, A. Polman, and R. Serna, Phys. Rev. B **49**, 16 313 (1994).
[4] F. Priolo, G. Franzò, S. Coffa, and A. Carnera, Phys. Rev. B **57**, 4443 (1998).
[5] J. Palm, F. Gan, B. Zheng, J. Michel, and L. C. Kimerling, Phys. Rev. B **54**, 17 603 (1996).
[6] F. Priolo, G. Franzò, S. Coffa, A. Polman, S. Libertino, R. Barklie, and D. Carey, J. Appl. Phys. **78**, 3874 (1995).
[7] I. Tsimperidis, T. Gregorkiewicz, H. H. P. Th. Bekman, and C. J. G. M. Langerak, Phys. Rev. Lett. **81**, 4748 (1998).
[8] T. Gregorkiewicz, D. T. X. Thao, J. M. Langer, H. H. P. Th. Bekman, M. S. Bresler, J. Michel, and L. C. Kimerling, Phys. Rev. B **61**, 5369 (2000).
[9] A. Taguchi and K. Takahei, J. Appl. Phys. **83**, 2800 (1998).
[10] A. Taguchi, K. Takahei, and Y. Horikoshi, J. Appl. Phys. **76**, 7288 (1994).
[11] P. G. Kik and A. Polman, J. Appl. Phys. **88**, 1992 (2000).
[12] K. Watanabe, S. Takeoka, M. Fujii, S. Hayashi, and K. Yamamoto, J. Lumin. **87**, 426 (2000).
[13] H. Przybylińska, W. Jantsch, Yu. Suprun-Belevitch, M. Stepikhova, L. Palmetshofer, G. Hendorfer, A. Kozanecki, R. J. Wilson, and B. J. Sealy, Phys. Rev. B **54**, 2532 (1996).
[14] W. Jantsch (private communication).
[15] F. Auzel, A. M. Jean-Louis, and Y. Toudic, J. Appl. Phys. **66**, 3952 (1989).
[16] M. S. Bresler, O. B. Gusev, B. P. Zakharchenya, and I. N. Yassievich, Phys. Solid State **38**, 813 (1996).
[17] I. N. Yassievich and L. C. Kimerling, Semicond. Sci. Technol. **8**, 718 (1993).
[18] A. Taguchi, K. Takahei, M. Matsuoka, and S. Tohno, J. Appl. Phys. **84**, 4471 (1998).
[19] V. N. Abakumov, V. I. Perel, and I. N. Yassievich, *Nonradiative recombination in semiconductors*, edited by V. M. Agranovich and A. A. Maradudin (North-Holland, Amsterdam, 1991), Vol. 33.
[20] T. Aitasalo, J. Hölsä, H. Jungner, M. Lastusaari, and J. Niittykoski, J. Lumin. **94-95**, 59 (2001).
[21] J. M. Langer, T. Langer, G. L. Pearson, B. Krukowska-Fulde, and U. Piekara, Phys. Status Solidi B **66**, 537 (1974).
[22] T. Gregorkiewicz, D. T. X. Thao, I. Tsimperidis, H. H. P. Th. Bekman, C. J. G. M. Langerak, J. Michel, and L. C. Kimerling, J. Lumin. **80**, 291 (1999).